The improved Amati correlations from Gaussian copula

YANG LIU, FUYONG CHEN, NAN LIANG, 2,3 ZUNLI YUAN, HONGWEI YU, AND PUXUN WU

¹ Department of Physics and Synergistic Innovation Center for Quantum Effects and Applications, Hunan Normal University, Changsha, Hunan 410081, China

² Key Laboratory of Information and Computing Science Guizhou Province, Guizhou Normal University, Guiyang, Guizhou 550025, China
³ Yunnan Observatory, Chinese Academy of Sciences, Kunming, Yunnan 650011, China

(Received; Revised; Accepted)

Submitted to

ABSTRACT

In this paper, we obtain two improved Amati correlations of the Gamma-Ray burst (GRB) data via a powerful statistical tool called copula. After calibrating, with the low-redshift GRB data, the improved Amati correlations based on a fiducial Λ CDM model with $\Omega_{\rm m0}=0.3$ and $H_0=70~{\rm km~s^{-1}Mpc^{-1}}$, and extrapolating the results to the high-redshift GRB data, we obtain the Hubble diagram of GRB data points. Applying these GRB data to constrain the Λ CDM model, we find that the improved Amati correlation from copula can give a result well consistent with $\Omega_{\rm m0}=0.3$, while the standard Amati and extended Amati correlations do not. This results suggest that when the improved Amati correlation from copula is used in the low-redshift calibration method, the GRB data can be regarded as a viable cosmological explorer. However, the Bayesian information criterion indicates that the standard Amati correlation remains to be favored mildly since it has the least model parameters. Furthermore, once the simultaneous fitting method rather than the low-redshift calibration one is used, there is no apparent evidence that the improved Amati correlation is better than the standard one. Thus, more works need to be done in the future in order to compare different Amati correlations.

1. INTRODUCTION

The accelerating cosmic expansion was first discovered by two independent teams in 1998 (Riess et al. 1998; Perlmutter et al. 1999) from observation of Type Ia supernova (SNIa). This discovery was further confirmed by many other observations, including the cosmic microwave background radiation (CMB) (Spergel et al. 2003, 2007) and the baryon acoustic oscillation (BAO) (Eisenstein et al. 2005). To explain this observational phenomenon, a mysterious dark energy has been proposed to exist in our universe. The nature of dark energy can be characterized by its equation of state (EoS) parameter. The simplest candidate of dark energy is the cosmological constant Λ , whose EoS parameter equals to -1, and the cosmological constant plus cold dark matter (Λ CDM) model is consistent with observational data very well. Based on the Λ CDM model, a tight constraint on the Hubble constant H_0 can be given with very high-redshift CMB data (Aghanim et al. 2019), which has a more than 4σ deviation from the value of H_0 obtained directly from the very low-redshift SNIa data (Riess et al. 2021, 2018a,b). Some other low-redshift observational data such as the Hubble parameter measurements H(z), BAO, and the strong gravitational lenses, have been used to explore the Hubble constant, and given a lower H_0 than the one from the SNIa with large error bars which are reasonably consistent with the value of Planck 2018 (Wu et al. 2017; Chen et al. 2017; Abbott et al. 2018; Birrer et al. 2020; Cao et al. 2021a; Lin & Ishak 2021; Khetan et al. 2021; Efstathiou 2020; Freedman 2021). The H_0 tension seems to suggest that the assumed Λ CDM model used to determine the Hubble constant may be inconsistent with our present universe or there are potentially unknown systematic errors in observational data. To precisely nail down the property of dark energy and the possible origin of H_0 tension, intermediate-redshift observational data are necessary, since the SNIa and BAO only contain the redshift ranges of $z \lesssim 2$ and the CMB is at $z \sim 1100$.

Gamma-Ray bursts (GRBs) are the most violent and intriguing explosions in the universe, whose power is dominant in the (sub-)MeV gamma-ray range (Klebesadel et al. 1973). The highest isotropic energy of GRBs can be up to 10^{54} erg and the detected redshift of GRBs reaches to $z \sim 9.4$. Thus, GRBs have the potential to be a farther tracker than SNIa to explore the cosmic evolution. Many empirical luminosity correlations which are relationships between

parameters of the light curves and/or spectra with the GRB luminosity or energy have been proposed to standardize GRB samples, such as the time lag-isotropic peak luminosity correlation $(\tau_{lag} - L_{iso})$ (Norris et al. 2000), the time variability-isotropic peak luminosity correlation $(V - L_{iso})$ (Fenimore & Ramirez-Ruiz 2000), the Amati correlation (see the Appendix A for the details) which connects the spectral peak energy in GRB cosmological rest-frame and the the isotropic equivalent radiated energy $(E_p - E_{iso})$ (Amati et al. 2002), the correlation between the spectral peak energy and the isotropic peak luminosity $(E_p - L_{iso})$ (Yonetoku et al. 2004)), the correlation between the spectral peak energy and the collimated-corrected energy $(E_p - E_\gamma)$ (Ghirlanda et al. 2004a), and so on. Moreover, the issue of whether these luminosity correlations are redshift dependent is investigated in (Basilakos & Perivolaropoulos 2008; Demianski et al. 2017; Wang et al. 2011; Li 2007; Lin et al. 2015, 2016; Khadka et al. 2021), and . For an example, Demianski et al. (2017) introduced a power-law function to describe the evolutionary function of the Amati correlation with redshift, and Wang et al. (2017) selected two redshift dependent formulas to parameterize the coefficients in the Amati correlation, which is called the extended Amati correlation in this paper (the details can be found in the Appendix B). Since the luminosity L_{iso} , the isotropic energy E_{iso} and the collimated-corrected energy E_{γ} in GRBs are cosmology-dependent, the Hubble diagram can be obtained from standardized GRB samples.

To use the GRBs as a cosmological probe, we need to calibrate GRB correlations. Let us point out here that the cosmology-dependent calibration method suffers the so-called *circularity problem* (Ghirlanda et al. 2006; Wang et al. 2015). To avoid this problem, a low-redshift method (Liang et al. 2008; Kodama et al. 2008; Wei & Zhang. 2009; Liang et al. 2010) to calibrate the GRB correlations in a cosmology-independent way was proposed, which uses other distance probes such as SNIa to calibrate the GRBs at low-redshifts and then extrapolates the results to high-redshifts to constrain the cosmological parameters. For this method, since the intrinsic dispersion of SNIa data is very much smaller than the GRB intrinsic dispersion, the SNIa data will dominate over the GRB data in a joint analysis of them on the cosmological constraints and so the resulting cosmological constraints are effectively from SNIa data. On the other hand, the simultaneous fitting or global fitting (Ghirlanda et al. 2004b; Li et al. 2008) limits the coefficients of the luminosity correlations and the parameters of cosmological models simultaneously from the observational GRB data. In (Khadka & Ratra 2020; Khadka et al. 2021), by simultaneously fitting cosmological and GRB Amati correlation parameters and using a number of different cosmological models, it has been found that the Amati correlation parameter values are independent of the cosmological model, which seems to mean that there is no circularity problem and that these GRB data sets are standardizable within the error bars. Up to now, the GRB data has been used widely to investigate different cosmological models (see recent Refs: Amati et al. 2019; Demianski et al. 2021; Cao et al. 2021b, 2022; Hu et al. 2021; Wang et al. 2021; Luongo & Muccino 2021).

In this work we aim to improve the Amati correlation which has been widely used in GRB cosmology. We introduce a powerful statistical tool called copula, which is a specialized tool developed in modern statistics to describe the complicated dependence structures between multivariate random variables. Copula has been widely used in various areas such as mathematical finance and hydrology in the past few decades. In recent years, it has gradually been recognized by the astronomical community as a very useful tool to analyze data. For example, Yuan et al. (2018) successfully determined the luminosity function of the radio cores in active galactic nuclei via copula, which is difficult to do if the traditional method is used, Koen (2009) studied, using copula, the correlation between the GRB peak energy and the associated supernova peak brightness, Benabed et al. (2009) proposed a new approximation for the low multipole likelihood of the CMB temperature, and Jiang et al. (2009) constructed a period-mass function for extrasolar planets. In addition, the copula likelihood function was constructed for the convergence power spectrum from the weak lensing surveys by Sato et al. (2010, 2011). Modeling bivariate astronomical data with copula instead of the conventional gaussian mixture method was proposed by Koen & Bere (2017). The copula function is also useful in the study of galaxy luminosity functions and the large scale structure fields of matter density (Takeuchi 2010; Takeuchi et al. 2013; Takeuchi & Kono 2020; Scherrer et al. 2010; Qin et al. 2020). Based on the 3-dimensional Gaussian copula, we propose, in this work, two improved Amati correlations and compare them with the standard Amati correlation and the extended Amati correlation by using the latest GRB samples (Khadka et al. 2021).

The frame of this paper is arranged as follows: Section 2 studies the issue of how to construct a 3-dimensional probability density function (PDF) through a Gaussian copula. Two improved Amati correlations are obtained in Section 3. In Section 4, a comparison between the improved Amati correlations and the (extended) Amati correlation is made by using both low-redshift calibration and simultaneous fitting methods. The conclusions are given in Section 5.

2. THE COPULA

Briefly speaking, copulas are functions that join or "couple" multivariate distribution functions to their onedimensional marginal distribution functions (Nelson 2006). Let x, y and z be three random variables, we use F(x), G(y) and W(z) to express their marginal cumulative distribution functions (CDFs) respectively, and H as the joint distribution function of the three variables. According to Sklar's theorem, if F, G and W are continuous, there exists a unique copula C such that

$$H(x, y, z; \boldsymbol{\theta}) = C(F(x), G(y), W(z); \boldsymbol{\theta}), \tag{1}$$

where θ denotes the parameters of the copula function C. Let $u \equiv F(x)$, $v \equiv G(y)$, and $q \equiv W(z)$, the joint probability density function (PDF) $h(x, y, z; \theta)$ can be obtained by

$$h(x, y, z; \boldsymbol{\theta}) = \frac{\partial^{3} H(x, y, z; \boldsymbol{\theta})}{\partial x \partial y \partial z}$$

$$= \frac{\partial^{3} C(u, v, q; \boldsymbol{\theta})}{\partial u \partial v \partial q} \frac{\partial u}{\partial x} \frac{\partial v}{\partial y} \frac{\partial q}{\partial z}$$

$$= c[u, v, q; \boldsymbol{\theta}] f(x) g(y) w(z), \tag{2}$$

where f(x), g(y) and w(z) are the marginal PDFs of x, y and z respectively, and $c(u, v, q; \theta)$ is the density function of C.

One obvious advantage of Eq. (1) is that by using copulas one can model the dependence structure and the marginal distributions separately. All the information on the dependence between the three variables is carried by the copula (see, e.g., Yuan et al. 2018). The next issue is to find a 3-dimension optimal copula function and estimate its parameters to describe the observed data in GRBs. The bivariate copulas are abundant and thus the 3-dimensional copula functions are abundant too since most of the 2-dimensional copula can be extended easily to the 3-dimensional case. Here we use the 3-dimensional Gaussian copula function with linear correlation coefficient $\theta = {\rho_1, \rho_2, \rho_3}$ to model our data, i.e.,

$$C(u, v, q; \boldsymbol{\theta}) = \Psi_3 \left[\Psi_1^{-1}(u), \Psi_1^{-1}(v), \Psi_1^{-1}(q); \boldsymbol{\theta} \right], \tag{3}$$

where Ψ_3 and Ψ_1 are the standard 3-dimensional Gaussian CDF and 1-dimension Gaussian CDF respectively, and Ψ_1^{-1} denotes the inverse of Ψ . The density function of the Gaussian copula can be obtained from

$$c(u, v, q; \boldsymbol{\theta}) = \frac{\partial^{3} \Psi_{3} \left[\Psi_{1}^{-1}(u), \Psi_{1}^{-1}(v), \Psi_{1}^{-1}(q); \boldsymbol{\theta} \right]}{\partial u \partial v \partial q}$$

$$= \frac{1}{\sqrt{\det \boldsymbol{\Sigma}}} \exp \left\{ -\frac{1}{2} \left[\boldsymbol{\Psi}^{-1} \left(\boldsymbol{\Sigma}^{-1} - \mathbf{I} \right) \boldsymbol{\Psi}^{-1} \right] \right\}, \tag{4}$$

where $\Psi^{-1} \equiv \left[\Psi^{-1}(u), \Psi^{-1}(v), \Psi^{-1}(q)\right]^T$, **I** stands for the identity matrix, and Σ^{-1} denotes the inverse of the covariance matrix Σ , which reads

$$\Sigma \equiv \begin{pmatrix} 1 & \rho_1 & \rho_2 \\ \rho_1 & 1 & \rho_3 \\ \rho_2 & \rho_3 & 1 \end{pmatrix}. \tag{5}$$

The conditional PDF of y denotes the probability of variable y when x and z are fixed, which can be expressed as:

$$g_y(y|x,z;\boldsymbol{\theta}) \equiv \frac{h(x,y,z;\boldsymbol{\theta})}{h_{xz}(x,z;\rho_2)} = \frac{c[u,v,q;\boldsymbol{\theta}]f(x)g(y)w(z)}{c[u,q;\rho_2]f(x)w(z)} = \frac{c[u,v,q;\boldsymbol{\theta}]}{c[u,q;\rho_2]}g(y), \tag{6}$$

where $h_{xz}(x, z; \rho_2)$ is constructed from a 2-dimensional Gaussian copula with the correlation coefficient being ρ_2 . If variable y obeys a Gaussian distribution with the standard deviation being σ_y , then g_y can be expressed as

$$g_y(y|x,z;\boldsymbol{\theta}) = \frac{1}{\sqrt{2\pi\sigma_{y|x,z}^2}} \exp\left[-\frac{1}{2}S(x,y,z;\boldsymbol{\theta})\right],\tag{7}$$

where

$$\sigma_{y|x,z}^{2} \equiv \frac{\sigma_{y}^{2} \left(1 - \rho_{1}^{2} - \rho_{2}^{2} - \rho_{3}^{2} + 2\rho_{1}\rho_{2}\rho_{3}\right)}{1 - \rho_{2}^{2}}.$$
(8)

In Eq. (7), $S(x, y, z; \theta)$ is unknown if the marginal distributions of variables x and z are undetermined. Due to that the variable y obeys the Gaussian distribution, the highest probability of y corresponds to $S(x, y, z; \theta) = 0$.

3. THE IMPROVED AMATI CORRELATION

Now, we use the copula function introduced in the above section to investigate the correlation between E_p and E_{iso} of GRBs. After using x, y and z to denote $\log \frac{E_p}{300 \text{keV}}$, $\log \frac{E_{iso}}{1 \text{erg}}$ and redshift z of GRBs, respectively, the marginal distribution of x, y and z need to be given in order to determine $S(x, y, z; \theta)$. We assume that two Gaussian distributions for $x = \log \frac{E_p}{300 \text{keV}}$ and $y = \log \frac{E_{iso}}{1 \text{erg}}$ are

$$f(x; \bar{a}_x, \sigma_x) = \frac{1}{\sqrt{2\pi}\sigma_x} e^{-\frac{(\bar{a}_x - x)^2}{2\sigma_x^2}}, \ g(y; \bar{a}_y, \sigma_y) = \frac{1}{\sqrt{2\pi}\sigma_y} e^{-\frac{(\bar{a}_y - y)^2}{2\sigma_y^2}}.$$
 (9)

Here \bar{a} and σ represent the mean value and the standard deviation of the Gaussian distribution respectively. And the CDFs of x, y, respectively, have the forms

$$F(x; \bar{a}_x, \sigma_x) = \int_{-\infty}^x f(\tilde{x}; \bar{a}_x, \sigma_x) d\tilde{x}, \ G(y; \bar{a}_y, \sigma_y) = \int_{-\infty}^y g(\tilde{y}; \bar{a}_y, \sigma_y) d\tilde{y}.$$
 (10)

We consider two different redshift distributions of GRB data:

• the first distribution is a special form with the PDF being $w(z) = ze^{-z}$ (Wang et al. 2017). Thus, the corresponding CDF is:

$$W(z) = 1 - e^{-z}(1+z). (11)$$

• the second CDF of GRB's redshift distribution is the empirical distribution (Dekking et al. 2005):

$$W_N(z) = \begin{cases} 0 & \text{if } z < z_1 \\ i/n & \text{if } z_i \le z < z_{i+1} \\ 1 & \text{if } z_n \le z \end{cases}, \tag{12}$$

where $\{z_1, z_2, \dots, z_n\}$ is an ordered list of redshifts of GRB data, which satisfies $z_1 \leq z_2 \leq \dots \leq z_n$, and n denotes the number of data.

Since the first distribution of redshift z of GRBs given in Eq. (11) is an assumed special form, we need to evaluate whether the redshift of observed GRB data obeys this form by using the Kolmogorov-Smirnov test (K-S test). The K-S test bases on the distance measure D which is defined to be

$$D = \max|W_N(z) - W(z)|,\tag{13}$$

where $W_N(z)$ and W(z) are the empirical and assumed CDFs of redshift distribution of GRBs respectively. Apparently, D represents the maximum deviation between two CDFs. In our K-S test, we set the significance level α to be $\alpha = 0.05$, where $\alpha \equiv 1 - P(\lambda_{\alpha})$ and $P(\lambda)$ is the Kolmogorov distribution

$$P(\lambda) = \sum_{i=-\infty}^{+\infty} (-1)^i \exp\left(-2i^2\lambda^2\right)$$
 (14)

obeyed by the Kolmogorov stochasticity parameter λ . Here $\lambda \equiv \sqrt{N}D$ and N is the number of data. Then, a critical value $D_{\alpha} = \frac{\lambda_{\alpha}}{\sqrt{N}} \simeq 0.09$ can be obtained, which means that if the data satisfies the assumed distribution, the probability that $D < D_{\alpha}$ is about 95%. Conversely, the probability that $D > D_{\alpha}$ is only 5%. If $D > D_{\alpha}$, the assumed distribution

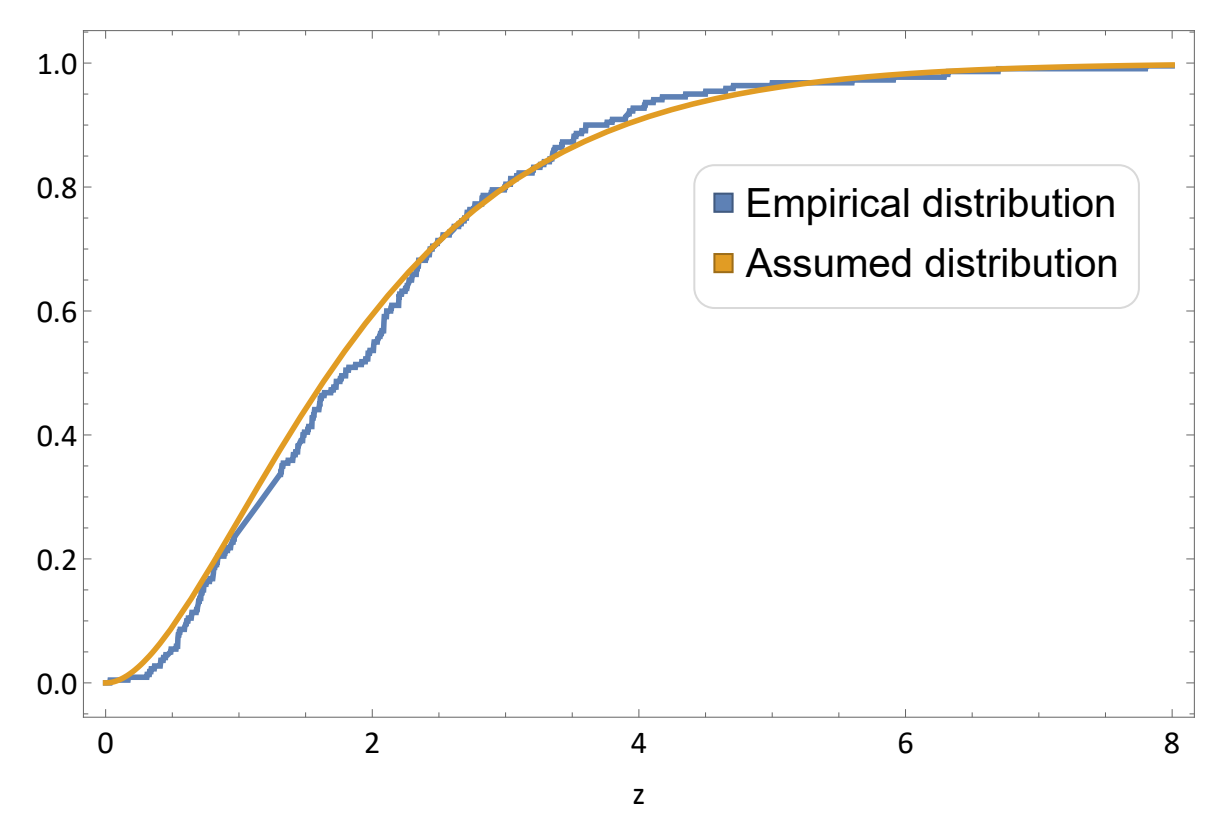


Figure 1. The CDFs of the empirical and assumed redshift distributions of GRB data. The maximum deviation between two CDFs is about 0.06 at $z \simeq 2$, and is less than the critical value $D_{\alpha} \simeq 0.09$, which means that the assumed distribution in our work passes the K-S test.

will be rejected since it is a rare event. Fig. 1 shows the CDFs of the empirical distribution $W_N(z)$ from the latest 220 GRB data points (Khadka et al. 2021) and the assumed distribution W(z) used in our discussion. We find that $D \simeq 0.06$ at $z \simeq 2$, which is less than D_{α} . Thus the assumed redshift distribution of GRB data passes the K-S test and is acceptable.

Substituting the CDFs given in Eqs. (10,11,12) into Eqs. (4-7), $S(x,y,z;\theta)$ can be derived. However, the concrete expression is very complicated, so we do not show it here. From the equation of $S(x,y,z;\theta) = 0$, we can obtain:

$$y_{\text{copula}_1} = a + b x + c \operatorname{erfc}^{-1}[2W(z)],$$

 $y_{\text{copula}_2} = a + b x + c \operatorname{erfc}^{-1}[2W_N(z)].$ (15)

Here, the subscripts copula₁ and copula₂ denote the correlation relations from the copula method with the assumed redshift distribution (Eq. (11)) and the empirical redshift distribution (Eq. (12)), respectively, erfc is the complementary error function, and coefficients a, b and c are defined as

$$a \equiv \bar{a}_{y} - \frac{(\rho_{2}\rho_{3} - \rho_{1}) \bar{a}_{x}\sigma_{y}}{(\rho_{2}^{2} - 1) \sigma_{x}},$$

$$b \equiv \frac{(\rho_{2}\rho_{3} - \rho_{1}) \sigma_{y}}{(\rho_{2}^{2} - 1) \sigma_{x}},$$

$$c \equiv \frac{\sqrt{2}\sigma_{y} (\rho_{3} - \rho_{1}\rho_{2})}{\rho_{2}^{2} - 1}.$$
(16)

Eq. (15) are different from the standard Amati correlation (Eq. (A1)) by a redshift-dependent term, and this redshift-dependent correction term is also different from that of the extended Amati correlation (Eq. (B14)). We name these luminosity correlations from the Gaussian copula as the improved Amati correlations, and they are the main results of our paper.

4. HUBBLE DIAGRAMS AND GRB COSMOLOGY

4.1. The low-redshift calibration

To test the viability of the improved Amati correlations given in Eq. (15), we use two GRB data samples: one is the latest GRB sample (A220) (Khadka et al. 2021), which contains 220 long GRBs in the redshift range of $z \in [0.03, 8.2]$, and the other is the higher-quality A118 data set (Khadka & Ratra 2020; Wang et al. 2016; Dirirsa et al. 2019) contained in A220 with redshift range of $z \in [0.34, 8.2]$ since it has a tighter intrinsic scatter. These GRBs are divided into the low-redshift part (79 and 20 GRBs at $z \in [0.1.4]$ in A220 and A118, respectively) and the high-redshift one (141 and 98 GRBs at $z \in [1.4, 8.2]$ in A220 and A118, respectively). We will use the low-redshift GRB data of two data sets to determine the coefficients in y_{copula} , and then extrapolate these results to the high redshift data to obtain their luminosity distances, which will then be used to constrain the cosmological model. Since the isotropic equivalent radiated energy E_{iso} (see Eq. (A4)) is dependent on the luminosity distance, a fiducial cosmological model needs to be chosen. Here, the spatially flat Λ CDM with $\Omega_{m0} = 0.30$ and $H_0 = 70$ km s⁻¹Mpc⁻¹ is chosen as the fiducial model, where Ω_{m0} is the dimensionless present matter density parameter. Then, the allowed regions of a, b, c and σ_{int} can be obtained by maximizing the D'Agostinis likelihood function

$$\mathcal{L}(\sigma_{int}, a, b, c) \propto \prod_{i=1}^{N} \frac{1}{\sqrt{\sigma_{int}^{2} + \sigma_{y,i}^{2} + b^{2}\sigma_{x,i}^{2}}} \times \exp\left[-\frac{[y_{i} - y_{\text{copula}}(x_{i}, z_{i}; a, b, c)]^{2}}{2\left(\sigma_{int}^{2} + \sigma_{y,i}^{2} + b^{2}\sigma_{x,i}^{2}\right)}\right].$$
(17)

Here N=79 or 20, σ_{int} is the intrinsic scatter of GRBs, and y_i denotes the observed $\log \frac{E_{iso}}{1 \mathrm{erg}}$ of the low-redshift GRBs. For a comparison, the Amati and extended Amati correlations, which are denoted by y_{Amati} and y_{exAmati} respectively, are also investigated. In our analysis, the CosmoMC code is used¹. The results are summarized in Tab. 1 and Tab. 2.

From two tables, one can see that in the case of the $copula_1$ correlation relation the value of intrinsic scatter σ_{int} is always slightly smaller than the one from the Amati relation, which means that the quality of the correlation relation is improved slightly when the $copula_1$ correlation relation is used. A comparison of Tab. 1 and Tab. 2 reveals that the value of intrinsic scatter σ_{int} from the A118 GRB data set is smaller than the one from the A220 GRB data set. Thus, the 118 data set is a higher quality one compared to the A220 data set, which agrees with the results obtained in (Khadka et al. 2021). Furthermore, Tab. 1 shows that the coefficient c in y_{copula_1} (or y_{copula_2}) and coefficients α and β in y_{exAmati} are at most 1σ away from 0, which indicates that there is not strong support for nonzero values of these parameters from the A220 data set. These results are consistent with what were obtained in (Khadka et al. 2021) where the relation parameters a and b were found to be independent of redshift within the error bars. This character may also be found from the Pearson linear correlation coefficients ρ_1 , ρ_2 and ρ_3 , which denote the degree of linear correlation between variables x, y and z. We derive $\rho_1 = 0.771$, $\rho_2 = 0.493$, $\rho_3 = 0.426$ from the 79 low-redshift GRBs in the A220 data set and $\rho_1 = 0.781$, $\rho_2 = 0.381$, $\rho_3 = 0.377$ from the 20 low-redshift GRBs in the A118 data set. Since ρ_2 and ρ_3 have values about 0.4 and they are smaller clearly than ρ_1 , the linear correlations between $\log \frac{E_p}{300 \mathrm{keV}}$ and z, and $\log \frac{E_p}{300 \text{keV}}$ and z are weak, and they are weaker than the linear correlation between $\log \frac{E_p}{300 \text{keV}}$ and $\log \frac{E_{so}}{1 \text{erg}}$. To compare the correlation relations from copula function and the (extended) Amati relation, we compute the values of the Akaike information criterion (AIC)(Akaike 1974, 1981) and the Bayesian information criterion (BIC)(Schwarz

$$AIC = 2p - 2\ln(\mathcal{L}),$$

$$BIC = p \ln N - 2\ln(\mathcal{L}),$$
(18)

where \mathcal{L} is the likelihood function, p is the number of free parameters in a model and N is the number of data. Here we also compute the $\Delta \text{AIC}(\Delta \text{BIC})$, which denotes the difference of AIC(BIC) with respect to the reference model (the standard Amati model here). $0 < \Delta \text{AIC}(\Delta \text{BIC}) \le 2$ indicates difficulty in preferring a given model, $2 < \Delta \text{AIC}(\Delta \text{BIC}) \le 6$ means mild evidence against the given model, and $\Delta \text{AIC}(\Delta \text{BIC}) > 6$ suggests strong evidence against the model. The obtained values of ΔAIC and ΔBIC are summarized in Tabs. 1 and 2. We find that except for the case of the extended Amati correlation whose ΔAIC given by the low-redshift GRBs in the A118 data set is

1978), which, respectively, are defined as:

¹ The CosmoMC code is available at https://cosmologist.info/cosmomc.

Table 1.

	Amati		extended Amati		copula	1	$copula_2$		
	$Best ext{-}fit(\sigma)$	0.68~CL	$Best ext{-}fit(\sigma)$	0.68~CL	$Best ext{-}fit(\sigma)$	0.68~CL	$Best ext{-}fit(\sigma)$	0.68~CL	
σ_{int}	$0.512(0.045)$ $^{+0.054}_{-0.034}$ $0.503(0.046)$ $^{+0.063}_{-0.025}$		0.510(0.045)	+0.054 -0.033	0.509(0.045)	+0.060 -0.029			
a	52.710(0.061)	$^{+0.060}_{-0.061}$	52.587(0.333)	$^{+0.324}_{-0.334}$	52.847(0.144)	$^{+0.145}_{-0.137}$	52.812(0.149)	$^{+0.141}_{-0.156}$	
b	1.290(0.126)	+0.126 -0.123	1.521(0.367)	$^{+0.422}_{-0.301}$	1.209(0.150)	$^{+0.145}_{-0.148}$	1.231(0.145)	$^{+0.156}_{-0.128}$	
c	_	_	_	_	-0.217(0.207)	$^{+0.208}_{-0.198}$	-0.142(0.192)	$^{+0.200}_{-0.180}$	
α	_	_	0.319(0.729)	$+0.734 \\ -0.702$	_	_	_	_	
β			-0.680(0.779)	$^{+0.624}_{-0.915}$	_	-	_	_	
$-2 \ln \mathcal{L}$	121.514		119.492		120.281		121.012		
$\Delta { m AIC}$	-		1.978		0.767		1.498		
$\Delta \mathrm{BIC}$	-	-		6.717		3.136		3.867	

NOTE—The best-fitted values, standard deviations, and the 68% confidence level (CL) of coefficients of y_{Amati} , y_{exAmati} , y_{copula_1} and y_{copula_2} from the 79 low-redshift (z < 1.4) long GRBs in A220 data set. Here $\Delta \text{AIC}(\Delta \text{BIC})$ denotes the difference of AIC(BIC) with standard Amati model.

Table 2.

	Amati		extended Amati		copula	1	$copula_2$		
	$Best ext{-}fit(\sigma)$	0.68~CL	$Best ext{-}fit(\sigma)$	0.68~CL	$Best ext{-}fit(\sigma)$	0.68~CL	$Best ext{-}fit(\sigma)$	0.68~CL	
σ_{int}	0.429(0.089)	$29(0.089)$ $^{+0.117}_{-0.044}$ $0.438(0.099)$ $^{+0.135}_{-0.041}$		0.418(0.098)	$^{+0.149}_{-0.025}$	0.430(0.097)	$^{+0.137}_{-0.035}$		
a	52.860(0.111)	$+0.105 \\ -0.110$	52.730(0.609)	+0.534 -0.6496	52.9586(0.282)	$^{+0.281}_{-0.257}$	52.935(0.282)	$^{+0.270}_{-0.266}$	
b	0.990(0.205)	$^{+0.210}_{-0.187}$	1.525(1.158)	$^{+1.230}_{-1.168}$	0.967(0.231)	$^{+0.213}_{-0.229}$	0.976(0.235)	$^{+0.218}_{-0.230}$	
c	_	_	_	_	-0.170(0.425)	$+0.394 \\ -0.423$	-0.103(0.368)	+0.339 -0.360	
α			0.329(1.327)	$^{+1.405}_{-1.170}$	_	_	_	_	
β			-1.136(2.270)	$^{+2.362}_{-2.476}$	_	_	_	_	
$-2 \ln \mathcal{L}$	23.374		22.938		23.119		23.240		
$\Delta { m AIC}$	-		3.564		1.745		1.866		
$\Delta \mathrm{BIC}$	-	-		5.555		2.741		2.862	

NOTE—The best-fitted values, standard deviations, and the 68% confidence level (CL) of coefficients of y_{Amati} , y_{exAmati} , y_{copula_1} and y_{copula_2} from the 20 low-redshift (z < 1.4) long GRBs in A118 data set.

larger than 2, the AIC cannot determine the model preferred by the data, while the BIC indicates that the standard Amati correlation remains to be favored mildly since it has the least model parameters.

Extrapolating directly the values of the coefficients in Tab. 1 and Tab. 2 from the low-redshift GRB data to the high-redshift samples we can construct the Hubble diagram of GRBs. The distance modulus of GRBs and their errors are obtained from Eqs. (A5) and (A10). As an example, in Fig. 2, we show the Hubble diagrams of 220 and 118 long GRBs obtained from three different correlations $(y_{\text{Amati}}, y_{\text{exAmati}})$ and y_{copula_1} , respectively. Here we do not plot the Hubble diagram based on the y_{copula_2} correlation since it is very similar to the one of y_{copula_1} . The values of distance modulus obtained from the copula method are less at low-redshift ($z \lesssim 1$) regions and larger at high-redshift ($z \gtrsim 1$) regions than the ones from the standard Amati correlation because a correction exists in the right hand side of Eq. (15).

To test whether the GRB can be regarded as the viable cosmological indicator, we can constrain the Λ CDM model from the distance modulus of GRBs obtained in the above subsection, and check whether $\Omega_{\rm m0} = 0.3$ is allowed after setting $H_0 = 70~{\rm km~s^{-1}Mpc^{-1}}$, which is used in calibrating the improved Amati correlations from the low redshift

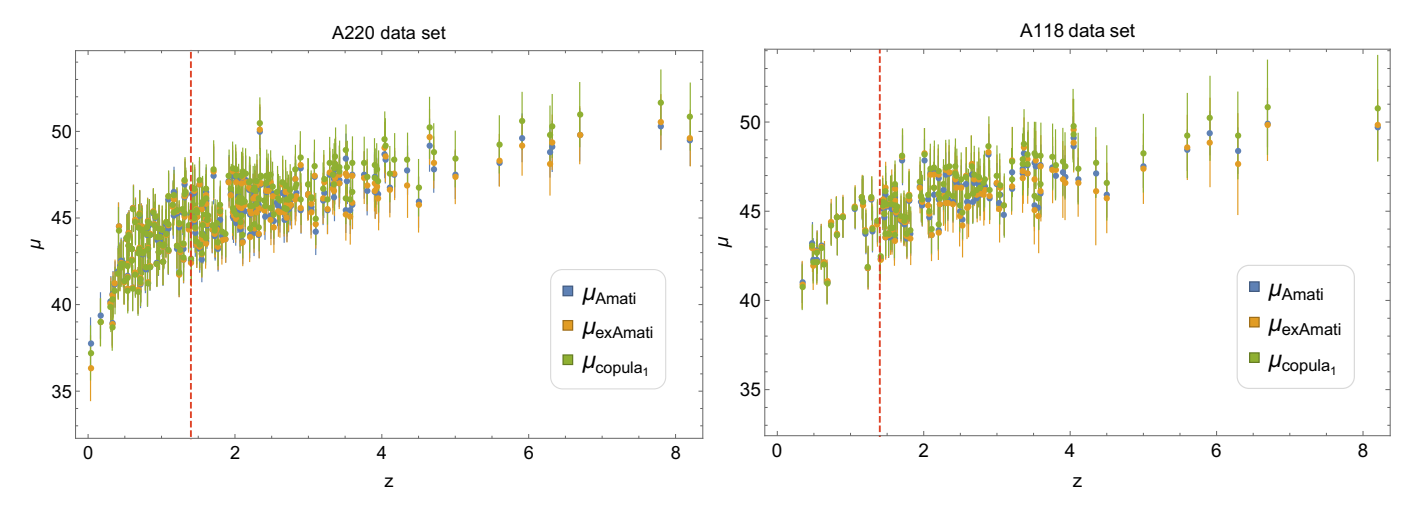


Figure 2. The Hubble diagrams of 220 and 118 long GRBs calibrated from three different correlations (y_{Amati} , y_{exAmati} and y_{copula_1}). The red dashed line denotes z = 1.4.

GRBs. The method of minimizing χ^2 is used to constrain $\Omega_{\rm m0}$. We consider two different samples for each data set: the 141 high-redshift GRBs and the total 220 GRBs for A220, and the 98 high-redshift GRBs and the total 118 GRBs for A118. We must emphasize here that since $W_N(8.2) = 1$ when the maximum redshift GRB data (z = 8.2) is considered, ${\rm erfc}^{-1}[2W_N(8.2)] = -\infty$ in y_{copula_2} and thus the data point with z = 8.2 will be ignored when the y_{copula_2} is used to constrain $\Omega_{\rm m0}$.

The probability density plots of Ω_{m0} for two data sets are shown in Fig. 3 and Fig. 4, and the best-fitted values with the standard deviation and 68% confidence level (CL) are summarized in Tab. 3 and Tab. 4, respectively. It is easy to see that for all data sets the results from the standard Amati correlation and the extended Amati correlation deviate apparently from $\Omega_{\rm m0} = 0.3$. The results from improved Amati correlation based on an empirical distribution of redshift (y_{copula_2}) are better than the ones from the (extended) Amati correlation although they are 1σ away from $\Omega_{\rm m0}=0.3$, while those from $y_{\rm copula_1}$ are always consistent with $\Omega_{\rm m0}=0.3$ at the 1σ confidence level. Apparently, the results from y_{copula_2} are not as good as those from y_{copula_1} . This is attributed to that the number of GRBs is still inadequate to construct the empirical distribution precisely. Comparing the constraint on Ω_{m0} from the high-redshift and full-redshift GRB data shown in Tabs. 3 and 4, we find that the values of $\Omega_{\rm m0}$ from the full-redshift data are closer to 0.3 than those from the high-redshift data. This is because the low-redshift data are calibrated with $\Omega_{\rm m0}=0.3$. When changing the GRB data from the high-redshift region to the full-redshift one, the A220 data give the maximum variation of $\Omega_{\rm m0}$ for the case of the extended Amati correlation, which is about 12%. However, this variation is very small at y_{copula_2} and y_{copula_2} cases. From Tabs. 3 and 4 and Figs. 3 and 4, one can also see that the values of Ω_{m0} from the total A220 data set are much closer to 0.3 than those from the full-redshift A118 data set. This is attributed to that the ratio of the number of the calibrated to the uncalibrated GRBs in the A220 data set, which is about 0.56 (79/141), is apparently larger than that in the A118 data set, which is only 0.20 (20/98). In addition, It is easy to find that our constraints on Ω_{m0} from the A118 and A220 data samples differ very significantly from what were obtained in (Khadka et al. 2021) where the A118 and A220 data limit $\Omega_{\rm m0} > 0.230$ and > 0.455, respectively, at the 95% CL in the Λ CDM model. This difference originates from that we utilize the low-redshift calibration method while the simultaneous fitting was used in (Khadka et al. 2021).

4.2. The simultaneous fitting

To show clearly the difference of the results from the GRB low-redshift calibration and the simultaneous fitting, now we follow the steps as in (Khadka et al. 2021; Cao et al. 2022) to use the simultaneous fitting method to constrain the cosmological parameter and the coefficients of four correlation relations. After setting $H_0 = 70 \text{ km s}^{-1}\text{Mpc}^{-1}$, the constraints on Ω_{m0} and the coefficients of four correlation relations can be obtained from the A118 and A220 data samples by using the D'Agostinis likelihood function (Eq. 17).

Fig. 5 shows one dimensional probability density plots and contour plots of $\Omega_{\rm m0}$ and the coefficients of four correlation relations, and the marginalized mean values with the standard deviation and the 68% CL are summarized in Tab. 5. We find that the results from the standard Amati correlation are slightly different from what were obtained in (Cao et

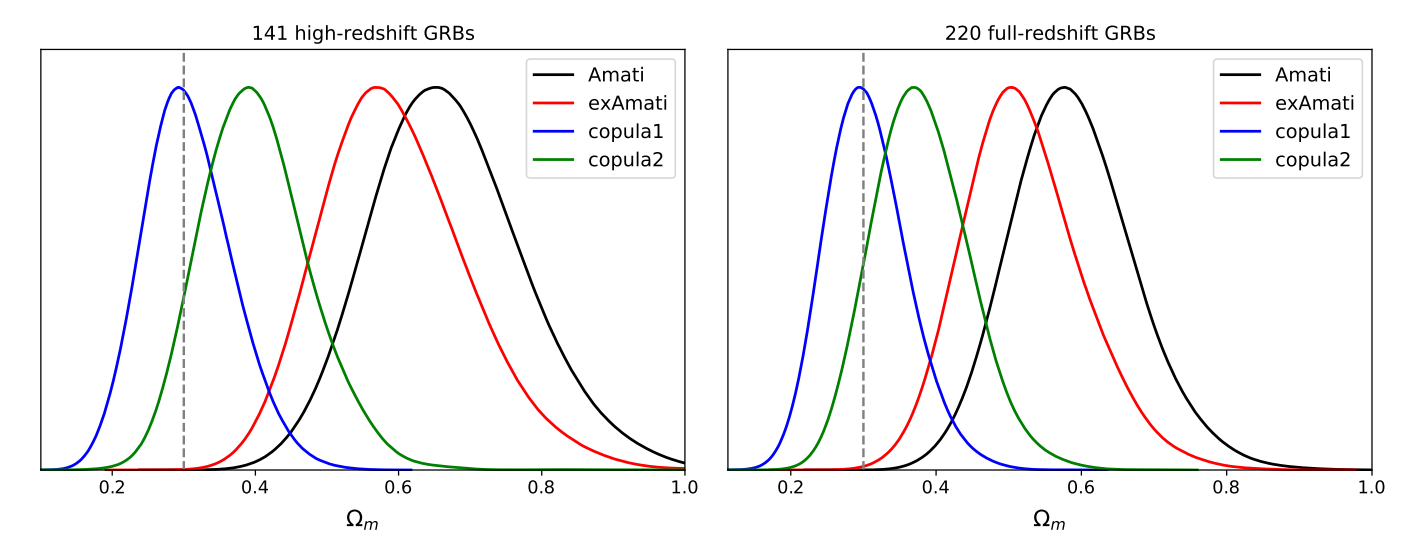


Figure 3. The probability density plots of $\Omega_{\rm m0}$ in the $\Lambda{\rm CDM}$ model with $H_0=70~{\rm km~s^{-1}Mpc^{-1}}$. The left and right panels show the results from the 141 high-redshift GRBs and full-redshift 220 GRBs, respectively. The gray dashed line denotes the $\Omega_{\rm m0}=0.3$ which is the value of fiducial model.

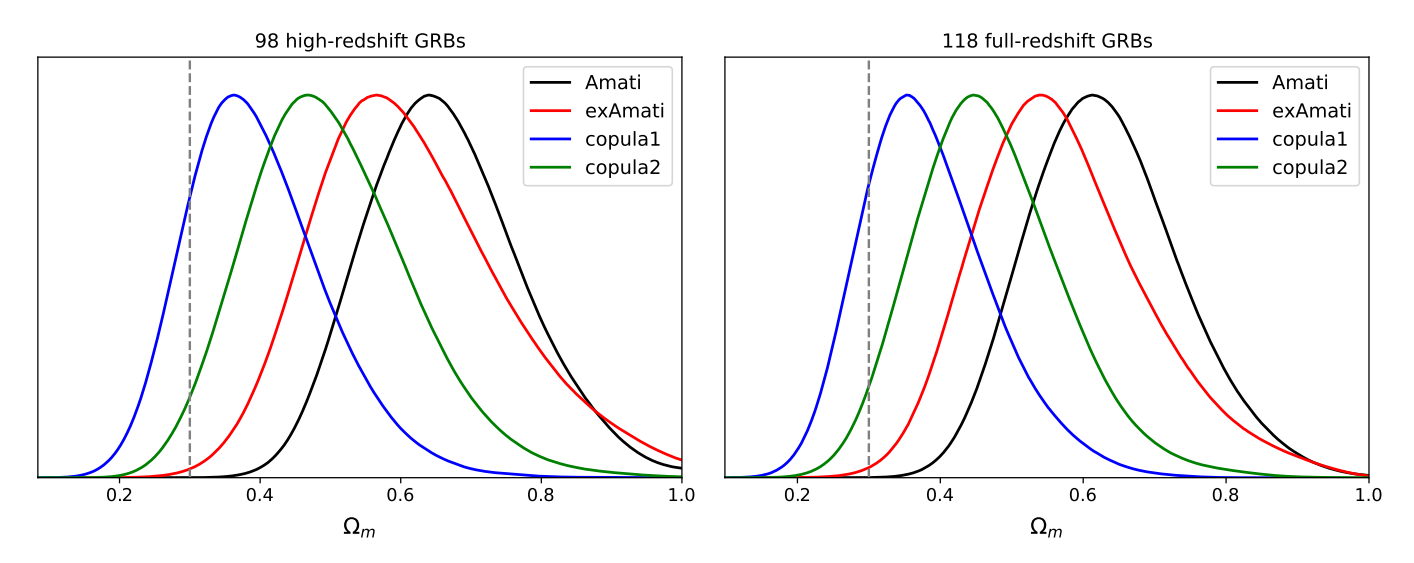


Figure 4. The probability density plots of $\Omega_{\rm m0}$ in the $\Lambda{\rm CDM}$ model with $H_0=70~{\rm km~s^{-1}Mpc^{-1}}$. The left and right panels show the results from the 98 high-redshift GRBs and full-redshift 118 GRBs, respectively. The gray dashed line denotes the $\Omega_{\rm m0}=0.3$ which is the value of fiducial model.

al. 2022). This is because the peak energy of the GRB 081121 data point, which is released in (Dirirsa et al. 2019) and used in (Cao et al. 2022), is different from the one given in Tab. 1 of (Amati et al. 2009), and it actually corresponds to the distance modulus rather than the peak energy in Tab. 4 of Wang et al. (2016)). Thus, there is an error in the peak energy of the GRB 081121 used in (Cao et al. 2022). If this error were not corrected, we would obtain the same result as Cao et al. (2022). In our analysis we have corrected this error. Comparing Tab. 5 and Tabs. 1 and 2, we find that the values of c from the simultaneous fitting are smaller and closer to zero than the ones from the low-redshift calibration. This seems to indicate that the evolutionary character with redshift of Amati correlation becomes weaker when more high redshift data are used. Fig. 5 and Tab. 5 show that when the simultaneous fitting method is used, the results from the improved Amati correlations are similar to those from the standard Amati correlation since the GRB data favor a large value of $\Omega_{\rm m0}$ and can only give a low bound limit on $\Omega_{\rm m0}$ although the low bound limits from the improved Amati correlations are smaller clearly than the one from the standard Amati correlation. If the extended Amati correlation is considered, there is almost no constraint on $\Omega_{\rm m0}$ from GRB, which should be attributed

Table 3.

	high-redshift				full-redshift				
	$\Omega_{\mathrm{m}0}(\sigma)$	$68\%\mathrm{CL}$	χ^2		$\Omega_{ m m0}(\sigma)$	$68\%\mathrm{CL}$	χ^2		
Amati	0.649(0.106)	+0.114 -0.096	90.535		0.589(0.086)	$^{+0.091}_{-0.077}$	168.851		
extend Amati	0.574(0.103)	$^{+0.107}_{-0.093}$	86.194		0.507(0.083)	$^{+0.083}_{-0.078}$	164.098		
$copula_1$	0.295(0.063)	$+0.067 \\ -0.057$	86.050		0.296(0.057)	$+0.058 \\ -0.053$	160.779		
$copula_2$	0.385(0.077)	$+0.080 \\ -0.068$	84.264		0.368(0.067)	+0.071 -0.060	159.941		

Note—The best-fitted value of $\Omega_{\rm m0}$ with the standard deviation σ and the 68% CL. The results are obtained from A220 data set.

Table 4.

	high	-redshift		full-redshift				
	$\Omega_{ m m0}(\sigma)$	$68\%\mathrm{CL}$	χ^2	$\Omega_{ m m0}(\sigma)$	$68\%\mathrm{CL}$	χ^2		
Amati	0.638(0.109)	+0.119 -0.100	69.710	0.607(0.105)	+0.116 -0.094	88.551		
extend Amati	0.579(0.133)	$^{+0.138}_{-0.123}$	50.431	0.540(0.120)	$^{+0.123}_{-0.108}$	66.905		
$copula_1$	0.390(0.101)	$+0.105 \\ -0.086$	46.979	0.381(0.094)	+0.099 -0.081	64.609		
$copula_2$	0.466(0.117)	$+0.130 \\ -0.097$	46.563	0.445(0.103)	$^{+0.110}_{-0.090}$	63.794		

NOTE—The best-fitted value of Ω_{m0} with the standard deviation σ and the 68% CL. The results are obtained from A118 data set.

to that this relation has more coefficients. Thus, once the simultaneous fitting method is used, we can not find that the improve Amati correlations obtained in this paper are apparently better than the standard and extended Amati correlations. These results are different significantly from those obtained in the subsection above with the low-redshift calibration method.

5. CONCLUSIONS

In this paper, we use the three dimensional Gaussian copula method to investigate the luminosity correlation of GRB data. By assuming that the logarithms of the special peek energy and the isotropic energy of GRBs satisfy the Gaussian distributions and two different redshift distributions of GRB data (one is the special form given in Eq. (11) and the other is empirical distribution), we obtain two improved Amati correlations of GRB data (y_{copula_1} and y_{copula_2}), which are distinctively different from the standard Amati correlation and the extended Amati correlation. After calibrating, with the low-redshift GRB data points from A220 and A118 data sets respectively, these improved Amati correlations based on a fiducial Λ CDM model with $\Omega_{\rm m0}=0.3$ and $H_0=70~{\rm km~s^{-1}Mpc^{-1}}$, and extrapolating the results to the high-redshift GRB data, we obtain the Hubble diagrams of 220 and 118 GRB data points. Applying these GRB data to constrain the Λ CDM model, we find that the results from the improved Amati correlations are apparently better than those from the standard Amati and extended Amati correlations although the BIC favors mildly the standard Amati correlation. The improved Amati correlation based on the special redshift distribution of GRB data gives the best result, which is always consistent with $\Omega_{\rm m0}=0.3$ at the 1σ confidence level and is highly consistent with $\Omega_{\rm m0} = 0.3$ when A220 data set is used. These results seem to indicate that when the improved Amati correlation with the special redshift distribution (y_{copula_1}) is used in the low-redshift calibration, the GRB data can be regarded as a viable cosmological explorer. However, the BIC indicates that the standard Amati correlation remains to be favored mildly since it has the least model parameters. Furthermore, once the simultaneous fitting method rather than the low-redshift calibration one is used, we find that the constraints on Ω_{m0} are weak and only the low bound limit on $\Omega_{\rm m0}$ can be obtained. Although this low bound limit from the improved Amati correlation is smaller than the one from the standard Amati correlation, there is no apparent evidence that the former is better than the latter. This

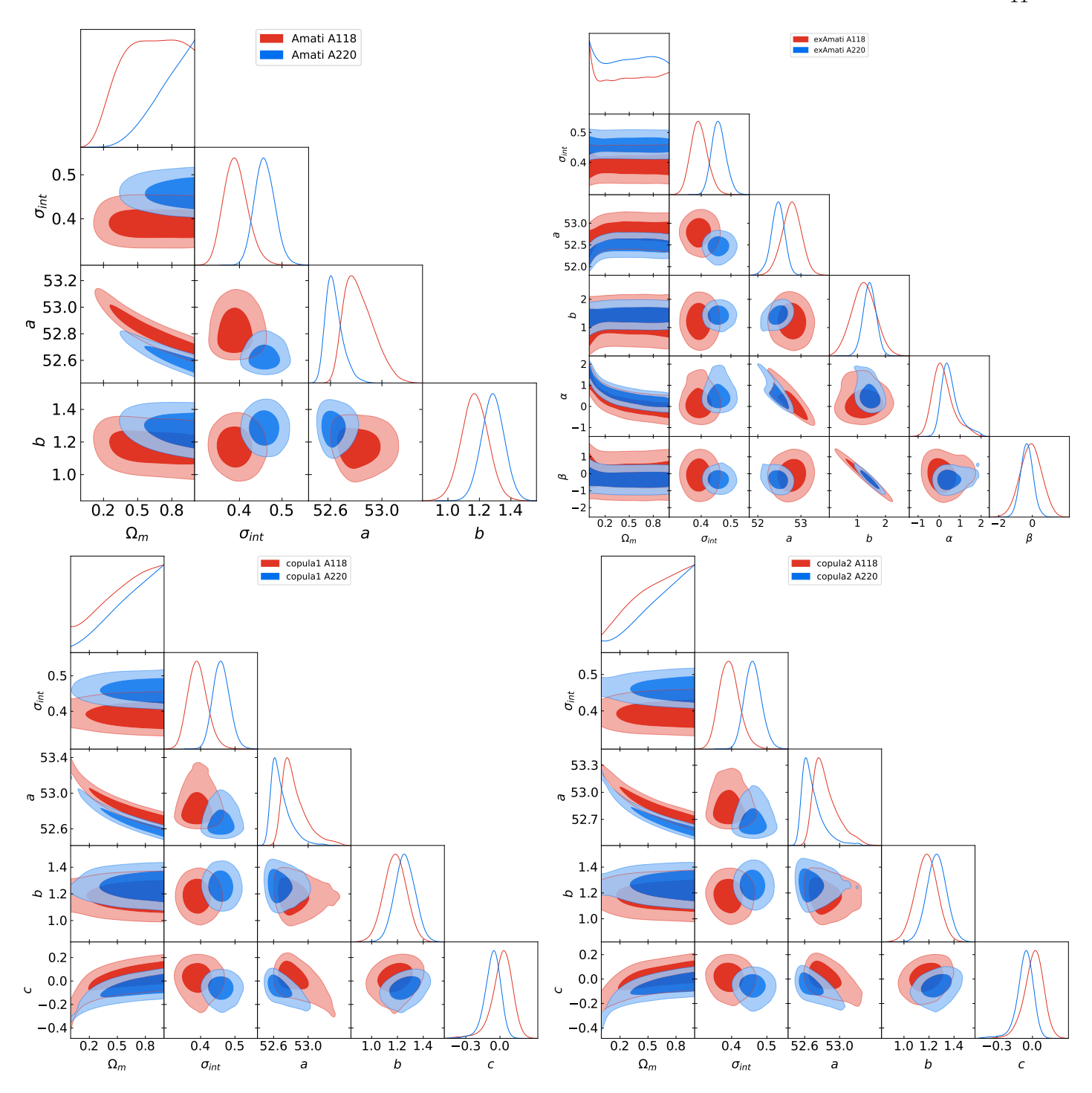


Figure 5. The results of simultaneously fitting the flat Λ CDM model and four correlations via the A118 (red) and A220 (blue) data sets. The upper left, upper right, lower left and lower right panels denotes the Amati, extended Amati, copula₁ and copula₂ correlations, respectively.

result is different apparently from the one from the low-redshift calibration method. Therefore, more works need to be done in the future in order to compare different Amati correlations.

Table 5.

Data set	Amati			extended A	extended Amati		1	$copula_2$	
		$Mean(\sigma)$	0.68~CL	$Mean(\sigma)$	0.68~CL	$Mean(\sigma)$	0.68~CL	$Mean(\sigma)$	0.68~CL
	$\Omega_{\mathrm{m}0}$	> 0.713	_	_	_	> 0.554	_	> 0.550	_
	σ_{int}	0.459(0.024)	$^{+0.022}_{-0.025}$	0.459(0.0.024)	$^{+0.021}_{-0.026}$	0.460(0.024)	$^{+0.022}_{-0.026}$	0.461(0.024)	$^{+0.022}_{-0.026}$
A220	a	52.630(0.068)	+0.045 -0.079	52.462(0.158)	+0.160 -0.140	52.685(0.118)	+0.052 -0.130	52.692(0.127)	$+0.048 \\ -0.140$
	b	1.286(0.072)	$^{+0.072}_{-0.072}$	1.434(0.228)	$^{+0.230}_{-0.230}$	1.258(0.078)	$^{+0.078}_{-0.078}$	1.262(0.079)	$^{+0.078}_{-0.078}$
	c	_	_	_	_	-0.066(0.074)	+0.077 -0.057	-0.064(0.075)	$^{+0.076}_{-0.052}$
	α	_	_	0.544(0.447)	$^{+0.240}_{-0.510}$	_	_	_	_
	β	_	_	-0.337(0.370)	$^{+0.370}_{-0.370}$	_	_	_	_
	$\Omega_{\mathrm{m}0}$	0.610(0.230)	$^{+0.340}_{-0.170}$	< 0.680	_	> 0.470	_	> 0.459	_
	σ_{int}	0.391(0.028)	$^{+0.024}_{-0.031}$	0.394(0.028)	$^{+0.024}_{-0.031}$	0.392(0.028)	$^{+0.025}_{-0.031}$	0.394(0.029)	$^{+0.025}_{-0.031}$
	a	52.826(0.115)	$^{+0.082}_{-0.140}$	52.786(0.228)	$^{+0.240}_{-0.210}$	52.846(0.147)	+0.067 -0.170	52.845(0.142)	+0.075 -0.170
A118	b	1.171(0.085)	$^{+0.085}_{-0.085}$	1.234(0.422)	$^{+0.418}_{-0.420}$	1.183(0.086)	$^{+0.086}_{-0.086}$	1.179(0.089)	$^{+0.089}_{-0.089}$
	c	_	_	_	_	0.017(0.097)	$^{+0.100}_{-0.068}$	0.010(0.084)	+0.089 -0.069
	α	_	_	0.198(0.520)	$^{+0.333}_{-0.587}$	_	_		_
	β	_	_	-0.097(0.629)	+0.626 -0.625	_	_	_	_

NOTE—The marginalized mean values, standard deviations, and the 68% CL of the flat Λ CDM model parameter and coefficients of $y_{\rm Amati}$, $y_{\rm exAmati}$, $y_{\rm copula_1}$ and $y_{\rm copula_2}$ from the A220 and A118 data set using the simultaneous fitting method.

ACKNOWLEDGMENTS

We appreciate very much the insightful comments and helpful suggestions by anonymous referees. This work was supported in part by the NSFC under Grants No. 12075084, No. 11690034, No. 11805063, No. 11775077, and 12073069, by the Science and Technology Innovation Plan of Hunan province under Grant No. 2017XK2019, and by the Guizhou Provincial Science and Technology Foundation (QKHJC-ZK[2021] Key 020).

APPENDIX

A. THE AMATI CORRELATION

In 2002, Amati et al. found that in GRB observational data there is a positive correlation between the spectral peak energy E_p and the isotropic equivalent radiated energy E_{iso} (Amati 2006a,b; Amati et al. 2008, 2009), and this correlation has the form

$$y_{\text{Amati}} = a + bx,\tag{A1}$$

where

$$y \equiv \log \frac{E_{iso}}{1 \text{erg}}, \ x \equiv \log \frac{E_p}{300 \text{keV}},$$
 (A2)

intercept a and slope b are free coefficients, "log" denotes the logarithm to base 10, and

$$E_p = E_p^{obs}(1+z), \tag{A3}$$

$$E_{iso} = 4\pi d_L^2(z) S_{bolo}(1+z)^{-1}.$$
 (A4)

Here z is the redshift, E_P^{obs} is the observed peak energy of GRB spectrum, $d_L(z)$ is the luminosity distance, and S_{bolo} is the bolometric fluence.

If the coefficients a and b are determined, the luminosity distance of GRB data point can be obtained from Eqs. (A1, A3, A4). Then we can obtain the distance modulus of GRB data, which is defined to be

$$\mu = 5 \log \frac{d_L(z)}{\text{Mpc}} + 25. \tag{A5}$$

If assuming a fiducial cosmological model, the values of coefficients a and b in the Amati correlation can be obtained from the observational data by using the following common fitting strategy (D'Agostini 2005):

$$\mathcal{L}(\sigma_{int}, a, b) \propto \prod_{i} \frac{1}{\sqrt{\sigma_{int}^2 + \sigma_{yi}^2 + b^2 \sigma_{xi}^2}} \times \exp\left[-\frac{(y_i - a - bx_i)^2}{2(\sigma_{int}^2 + \sigma_{yi}^2 + b^2 \sigma_{xi}^2)}\right],\tag{A6}$$

where σ_x and σ_y are the uncertainties of x and y, respectively, and σ_{int} is the intrinsic uncertainty of GRB. From the well-known error propagation equation, one find that σ_y and σ_x can be derived from Eqs. (A3,A4) and have the expressions:

$$\sigma_y = \frac{1}{\ln 10} \frac{\sigma_{E_{iso}}}{E_{iso}}, \ \sigma_x = \frac{1}{\ln 10} \frac{\sigma_{E_p}}{E_p}$$
 (A7)

with

$$\sigma_{E_{iso}} = 4\pi d_L^2 \sigma_{S_{bolo}} (1+z)^{-1}.$$
 (A8)

Here σ_{E_p} and $\sigma_{S_{bolo}}$ are available in observations of GRBs. Therefore, maximizing the likelihood function \mathcal{L} (Eq. A6), the allowed values of a, b, and σ_{int} can be obtained. Then the covariance matrix C_{ij} of these fitted parameters can be approximately evaluated from:

$$(C^{-1})_{ij}(\boldsymbol{\theta}_A) = \frac{\partial^2 [-\ln \mathcal{L}(\boldsymbol{\theta}_A)]}{\partial \theta_i \partial \theta_j} |_{\boldsymbol{\theta}_A = \boldsymbol{\theta}_b}, \tag{A9}$$

where $\theta_A = {\sigma_{int}, a, b}$, and θ_b denote the best-fitted value of a, b and σ_{int} .

Using the best fitted values of a and b, we can get the luminosity distance of GRBs and the corresponding distance modulus from Eq. (A5). By using the error propagation equation, the uncertainty of distance modulus can be derived from the following equation

$$\sigma_{\mu}^{2} = \left(\frac{5}{2}\sigma_{\log\frac{E_{iso}}{1\text{erg}}}\right)^{2} + \left(\frac{5}{2\ln 10}\frac{\sigma_{S_{bolo}}}{S_{bolo}}\right)^{2}.$$
(A10)

Here

$$\sigma_{\log \frac{E_{iso}}{1 \text{erg}}}^{2} = \sigma_{a}^{2} + \left(\sigma_{b} \log \frac{E_{p}}{300 \text{keV}}\right)^{2} + 2 \sum_{i=1}^{3} \sum_{j=i+1}^{3} \left(\frac{\partial y_{\text{Amati}}(x; \boldsymbol{\theta}_{A})}{\partial \theta_{i}} \frac{\partial y_{\text{Amati}}(x; \boldsymbol{\theta}_{A})}{\partial \theta_{j}}\right) C_{ij} + \left(\frac{b}{\ln 10} \frac{\sigma_{E_{p}}}{E_{p}}\right)^{2} + \sigma_{int}^{2}.$$
(A11)

According to the distance modulus of GRBs, the cosmological model can be constrained by minimizing χ^2

$$\chi^{2} = \sum_{i=1}^{N} \left[\frac{\mu_{obs}(z_{i}) - \mu_{th}(z_{i}; p)}{\sigma_{\mu_{i}}^{obs}} \right]^{2}, \tag{A12}$$

where μ_{obs} is the distance modulus of GRB and $\mu_{th}(z_i; p)$ is the theoretic value of distance modulus in cosmological model with p representing the model parameters.

B. THE EXTENDED AMATI CORRELATION

The extended Amati correlation was proposed in (Wang et al. 2017) where the authors used two formulas to parameterize the coefficients a and b in the standard Amati correlation:

$$a \to A = a + \alpha \frac{z}{1+z}, \ b \to B = b + \beta \frac{z}{1+z},$$
 (B13)

where α and β are two constants. Substituting these parameterized formulas into the Eq. (A1), the extended Amati correlation can be obtained

 $y_{\text{exAmati}} = \left(a + \alpha \frac{z}{1+z}\right) + \left(b + \beta \frac{z}{1+z}\right)x.$ (B14)

Recently, Khadka et al. (2021) used the A220 GRB data set to limit α and β , and found that the Amati correlation is independent of redshift within the error bars. The coefficient $\boldsymbol{\theta}_{ex} = \{\sigma_{int}, a, b, \alpha, \beta\}$ is also estimated from D'Agostinis likelihood function. The uncertainty of $\log \frac{E_{iso}}{\log \alpha}$ in Eq. (A10) can be obtained from

$$\sigma_{\log \frac{E_{iso}}{1 \text{erg}}}^{2} = \sigma_{a}^{2} + \left(\sigma_{b} \log \frac{E_{p}}{300 \text{keV}}\right)^{2} + \left(\sigma_{\alpha} \frac{z}{1+z}\right)^{2} + \left(\sigma_{\beta} \frac{z}{1+z} \log \frac{E_{p}}{300 \text{keV}}\right)^{2}$$

$$+ 2 \sum_{i=1}^{5} \sum_{j=i+1}^{5} \left(\frac{\partial y_{\text{exAmati}}(x; \boldsymbol{\theta}_{ex})}{\partial \theta_{i}} \frac{\partial y_{\text{exAmati}}(x; \boldsymbol{\theta}_{ex})}{\partial \theta_{j}}\right) C_{ij}$$

$$+ \left[\left(b + \beta \frac{z}{1+z}\right) \frac{1}{\ln 10} \frac{\sigma_{E_{p}}}{E_{p}}\right]^{2} + \sigma_{int}^{2}.$$
(B15)

REFERENCES

Abbott, T. M. C., et al. 2018, MNRAS, 480, 3879

Aghanim, N., et al. 2020, A&A, 641, A1

Akaike, H. 1974, IEEE Trans. Autom. Control., 19, 716

Akaike, H. 1981, J. Econom., 16,3

Amati, L., et al. 2002, A&A, 390, 81

Amati, L. 2006a, Nuovo Cimento B, 121, 1081

Amati, L. 2006b, MNRAS, 372, 233

Amati, L., et al. 2008, MNRAS, 391, 577

Amati, L., D'Agostino, R., Luongo, O., Muccino, M., & Tantalo, M. 2019, MNRAS, 486, L46

Amati, L., Frontera, F., & Guidorzi, C. 2009, A&A, 508, 173

Basilakos, S., & Perivolaropoulos, L., 2008, MNRAS, 391,

Benabed, K., Cardoso, J.-F., Prunet, S., & Hivon, E. 2009, MNRAS, 400, 219

Birrer, S., et al. 2020, A&A, 643, A165

Cao, S., Khadka, N., & Ratra, B. 2022, MNRAS, 510, 2928

Cao, S., Ryan, J., & Ratra, B. 2021a, MNRAS, 504, 300

Cao, S., Ryan, J., Khadka, N., & Ratra, B. 2021b, MNRAS, 501, 1520

Chen, Y., Kumar, S., & Ratra, B. 2017, ApJ, 835, 86

D'Agostini, G. 2005, arXiv:physics/0511182

Dekking, F. M., et al., A Modern Introduction to Probability and Statistics. London, U.K.: Springer-Verlag, 2005 Demianski, M., Piedipalumbo, E., Sawant, D., & Amati, L. 2017, A&A, 598, A112

Demianski, M., Piedipalumbo, E., Sawant, D., & Amati, L. 2021, MNRAS, 506, 903

Dirirsa, F. F, et al. 2019, ApJ, 887, 13

Efstathiou, G. 2020, arXiv:2007.10716v2

Eisenstein, D. J., et al. 2005, ApJ, 633, 560.

Fenimore, E. E., & Ramirez-Ruiz, E. 2000, arXiv:astro-ph/0004176

Freedman, W. L. 2021, ApJ, 919, 16

Ghirlanda, G., Ghisellini, G., & Lazzati, D. 2004a, ApJ, 616, 331

Ghirlanda, G., Ghisellini, G., Lazzati, D., & Firmani, C. 2004b, ApJ, 613, L13

Ghirlanda, G., Ghisellini, G., & Firmani, C. 2006, New, J. Phys., 8, 123

Hu, J. P., Wang, F. Y., & Dai, Z. G. 2021, MNRAS, 507, 730

Jiang, I.-G., Yeh, L.-C., Chang, Y.-C., & Hung, W.-L. 2009, AJ, 137, 329

Khadka, N., Luongo, O., Muccino, M., & Ratra, B. 2021, JCAP, 09, 042

Khadka, N., & Ratra, B. 2020, MNRAS, 499, 391

Khetan, N., et al. 2021, A&A, 647, A72

Klebesadel, R. W., Strong, I. B., & Olson, R. A. 1973, ApJ, 182, L85

Kodama, Y., et al. 2008, MNRAS, 391, L1

Koen, C. 2009, MNRAS, 393, 1370

Koen, C., & Bere, A. 2017, MNRAS, 471, 2771

Li, L.-X. 2007, MNRAS, 379, L55

Li, H. et al. 2008, ApJ, 680, 92

Liang, N., Xiao, W. K., Liu, Y., & Zhang, S. N. 2008, ApJ, 685, 354

Liang, N., Wu, P. & Zhang, S. N. 2010, PhRvD, 81, 083518Lin, H.-N., Li, X., Wang, S., & Chang, Z. 2015, MNRAS, 453, 128

Lin, H.-N., Li, X., Chang, Z. 2016, MNRAS, 455, 2131

Lin, W., & Ishak, M. 2021, JCAP, 05, 009

Luongo, O., & Muccino, M. 2021, arXiv:2110.14408

Nelson, R. B. 2006, An Introduction to Copulas (2nd ed.; New York: Springer)

Norris, J. P., Marani, G. F., & Bonnell, J. T. 2000, ApJ, 534, 248

Perlmutter, S., et al. 1999, ApJ, 517, 565

Qin, J., Yu, Y., & Zhang, P. 2020, ApJ, 897, 105

Riess, A. G., et al. 1998, AJ, 116, 1009

Riess, A. G., et al. 2018a, ApJ, 853, 126

Riess, A. G., et al. 2018b, ApJ, 861, 126

Riess, A. G., et al. 2021, ApJL, 908, L6

Sato, M., Ichiki, K., & Takeuchi, T. T. 2010, PhRvL, 105, 251301

Sato, M., Ichiki, K., & Takeuchi, T. T. 2011, PhRvD, 83, 023501

Scherrer, R. J., Berlind, A. A., Mao, Q., & McBride, C. K. 2010, ApJL, 708, L9

Schwarz, G. 1978, Annals of Stats, 6, 461

Spergel, D. N., et al. 2003, ApJS, 148, 175

Spergel, D. N., et al. 2007, ApJS, 170, 377

Takeuchi, T. T. 2010, MNRAS, 406, 1830

Takeuchi, T. T., & Kono, K. T. 2020, MNRAS, 498, 4365

Takeuchi, T. T., Sakurai, A., Yuan, F.-T., Buat, V., & Burgarella, D. 2013, Earth Planet Sp, 65, 281

Wang, F. Y., Dai, Z. G., & Liang, E. W. 2015, New Astronomy Reviews, 67, 1

Wang, F. Y., Hu, J. P., Zhang, G. Q., & Dai, Z. G. 2022, ApJ, 924, 97

Wang, F.-Y., Qi, S., & Dai, Z.-G. 2011, MNRAS, 415, 3423
Wang, G.-J., Yu, H., Li, Z.-X., Xia, J.-Q., & Zhu Z.-H.
2017, ApJ, 836, 103

Wang, J. S., Wang, F. Y., Cheng, K. S. & Dai, Z. G. 2016, A&A, 585, A68

Wei, H., Zhang, S. N. 2009, Eur. Phys. J. C, 63, 139
Wu, P.-X, Li, Z.-X, & Yu, H.-W. 2017, Front. Phys. 12, 129801

Yonetoku, D., et al. 2004, ApJ, 609, 935

Yuan, Z., Wang, J., Worrall, D. M., Zhang, B.-B., & Mao, J. 2018, ApJS, 239, 33